Microelectronics Journal 109 (2021) 104987

Contents lists available at ScienceDirect

Microelectronics Journal

journal homepage: www.elsevier.com/locate/mejo

The mining method of anti-electromagnetic interference for electronic equipment in coal mine by considering network communication technology

Yapeng Yan [a,b,*], Wentao Cao [a]

[a] Department of Mining Engineering, Yuncheng Vocational and Technical University, Yuncheng, China
[b] Shanxi Xiangning Coking Coal Group Tonghe Coal Industry Co., Ltd., Linfen, China

ARTICLE INFO

Keywords:
Network communication technology
Underground electronic equipment in coal mine
Anti-electromagnetic interference
Mining

ABSTRACT

It is impossible to analyze the harmonic interference source due to the influence of electromagnetic sensitivity when the original mining method of anti-electromagnetic interference for electronic equipment in coal mine is used., there is a problem of low wireless transmission rate of underground data. Therefore, a kind of mining method of anti-electromagnetic interference for electronic equipment in coal mine considering network communication technology is proposed to prevent electromagnetic interference, provide technical support for coal mine safety production. Firstly, harmonic interference source analysis is carried out, including harmonic analysis, input side interference source analysis and output side interference source analysis. Then the over-voltage of the motor terminal is carried out. The specific steps include using the cable transmission line model with distributed parameters to simulate the voltage of the motor terminal, and analyzing the voltage reflection process. Finally, based on the network communication technology, the supporting equipment of the comprehensive mining face is designed to realize the anti-electromagnetic interference mining of the underground electronic equipment. The experiment results show that the wireless transmission rate of underground data of the presented method is higher than that of the two original methods, and the rate is improved.

1. Introduction

There is a large number of mobile or semi-mobile production equipment in the mine, such as electric locomotive, electric haulage shearer, belt conveyor, etc. Large electromechanical equipment has high power, relatively concentrated position and frequent start and stop, which will produce serious electromagnetic interference and adversely affect the work of automation equipment such as communication in coal mine [1]. With the rapid development of power electronic technology and the integration of power equipment, various new power electronic equipments have appeared in coal mines. With higher switching frequency and power, the control circuit becomes more and more complex. In the process of high-speed switching, the power switching devices in the main circuit of these power electronic equipment will produce high dv/dt and di/dt, which will produce serious conducted electromagnetic interference and sometimes strong electromagnetic radiation, which will cause interference to underground mining work and even bring potential safety hazards [2]. Electromagnetic interference there will have a serious impact on the surrounding electronic and electrical equipment, and may endanger the safety of mining personnel. In addition, most of these down hole electronic devices use PWM technology, and the power spectrum of output voltage and current is discrete, which will produce a large number of high-order harmonic components related to switching frequency, causing electromagnetic pollution to the power grid. At the same time, the measurement and control circuits of these power electronic devices are also subject to electromagnetic interference from their main circuits and mine environment. Therefore, studying the anti-electromagnetic interference performance of electronic equipment in coal mines can realize non-interference, high-efficiency and safe mining in coal mines.

However, the research on anti-electromagnetic interference mining of coal mine electronic equipment at home and abroad is still in the development stage. At present, research on anti-electromagnetic interference of coal mine electronic equipment mainly focuses on electromagnetic interference testing technology, electromagnetic interference mechanism research, electromagnetic interference modeling, electromagnetic interference suppression technology and other directions. Some scholars have put forward a mining method for anti-

* Corresponding author. Department of Mining Engineering, Yuncheng Vocational and Technical University, Yuncheng, China.
E-mail addresses: yyp_13453777757@163.com (Y. Yan), LI15129182922@163.com (W. Cao).

https://doi.org/10.1016/j.mejo.2020.104987
Received 7 October 2020; Received in revised form 27 December 2020; Accepted 29 December 2020
Available online 23 January 2021

electromagnetic interference of coal mine electronic equipment based on electric field shielding technology, which mainly uses electric field shielding technology to suppress the influence of electrostatic field and constant magnetic field of coal mine electronic equipment, and eliminate the interference caused by distributed capacitive coupling among multiple circuits, so as to carry out the mining work smoothly [3]. Domestic research on anti-electromagnetic interference mining methods of underground electronic equipment is mainly about the propagation characteristics of electromagnetic waves, such as the influence of the shape and size of underground roadway on electromagnetic wave propagation, which mainly involves the influence of electromagnetic wave cut-off frequency in mine environment [4]. Some scholars put forward an anti-electromagnetic interference mining method for electronic equipment in coal mine based on single-point grounding technology, which mainly uses single-point grounding technology to connect all circuits and grounding wires of electronic equipment in coal mine to a common grounding point, and takes this point as the zero potential reference point of circuits and equipment, thus realizing anti-electromagnetic interference mining of electronic equipment in coal mine [5]. Due to the influence of electromagnetic sensitivity, it is impossible to analyze harmonic interference sources when using the above-mentioned mining method for anti-electromagnetic interference of underground electronic equipment. The transmission time of output pulse is in the range of 0.5 μs–1.1 μs, and the rate is low. Therefore, a mining method for anti-electromagnetic interference of electronic equipment in coal mine underground considering network communication technology is proposed, By analyzing the interference source of harmonic, calculating the total distortion rate of harmonic, simulating the voltage of motor terminal, analyzing the process of voltage reflection.

2. Design of the mining method of anti-electromagnetic interference for underground electronic equipment in coal mine considering network communication technology

There are many devices that generate and break high voltage and high current in coal mines, and their starting and working processes have strong interference on data transmission. Among the interference sources, harmonic interference, input impedance and output pulse voltage interference of frequency converter, distribution parameters of transmission lines, voltage reflection of motor terminals, etc.

2.1. Analysis of harmonic interference source

2.1.1. Harmonic analysis

By analyzing various possibilities of spectral line distribution near discrete frequency points of windowed signal, six spectral lines close to peak spectral line frequency points are used for calculation, and harmonic information contained in these spectral lines is fully considered. Multi-spectral line interpolation algorithm and modified fitting process are derived in detail, and the influence of harmonics on electromagnetic interference resistance of electronic equipment is studied. The ideal underground power grid of coal mine should provide sine wave voltage with single fixed frequency, specified voltage amplitude and phase number for electronic equipment:

$$u(t) = \sqrt{2}U\ \sin(\omega t + \varphi_u) \tag{1}$$

In equation (1), $u(t)$ represents the sine wave voltage with a single fixed frequency, specified voltage amplitude and phase number; U represents the effective value of the voltage; φ_u represents the initial phase angle of the voltage; t represents the sine wave; ω represents the angular frequency of the power supply, and its calculation equation is as follows:

$$\omega = \frac{2\pi}{T} \tag{2}$$

In equation (2), T represents period.

When the load of sine wave voltage is nonlinear, the voltage and current generated by the load may be non sinusoidal. Let the function $u(t)$ with period T satisfy the Dirichlet condition on interval $[-\frac{T}{2}, \frac{T}{2}]$:

At most, $u(t)$ has finite first type breakpoints, and $[-\frac{T}{2}, \frac{T}{2}]$ can be divided into finite partial intervals, so that $u(t)$ is monotone in each partial interval, then $u(t)$ can be expanded into complete orthogonal trigonometric function on this interval, as follows:

$$u(t) = \{1, \cos\frac{2\pi t}{T}, \cos\frac{4\pi t}{T}, ..., \cos\frac{2n\pi t}{T}, ..., \sin\frac{2\pi t}{T}, \sin\frac{4\pi t}{T}, ..., \sin\frac{2n\pi t}{T}\} \tag{3}$$

In equation (3), n represents a positive integer [6].

Its Fourier series is:

$$u(\omega t) = a_0 + \sum_{n-1}^{\infty}(a_n\ \cos\ n\omega t + b_n\ \sin\ n\omega t) \tag{4}$$

In equation (4), a_0 represents voltage signal; a_n represents periodic voltage signal; b_n represents periodic current signal, and their calculation equation is shown in equation (5).

$$\begin{cases} a_0 = \dfrac{1}{2\pi}\displaystyle\int_0^{2\pi} u(\omega t)d(\omega t) \\ a_n = \dfrac{1}{\pi}\displaystyle\int_0^{2\pi} u(\omega t)\cos\ n\omega t d(\omega t) \\ b_n = \dfrac{1}{\pi}\displaystyle\int_0^{2\pi} u(\omega t)\sin\ n\omega t d(\omega t) \\ n = 1,2,3... \end{cases} \tag{5}$$

In equation (5), d represents the fundamental frequency component.

It can be seen from the above equation that periodic voltage or current signal can be decomposed into the sum of DC component, fundamental component of frequency as equation (6) and harmonic component of integral multiple fundamental frequency component with frequency greater than 1 [7].

$$f = \frac{1}{T} \tag{6}$$

In equation (6), f represents frequency.

For harmonic voltage, the $n-th$ harmonic voltage content is:

$$HRU_n = \frac{U_n}{U_1} \times 100\% \tag{7}$$

In equation (7), HRU_n represents the $n-th$ harmonic voltage content; U_n represents the effective value of the $n-th$ harmonic voltage, and its calculation equation is shown in equation (8); U_1 represents the effective value of the fundamental voltage.

$$U_n = \sqrt{a_n^2 + b_n^2} \tag{8}$$

The total distortion rate of harmonic voltage is:

$$\begin{cases} THD = \dfrac{\sqrt{U_1^2 + U_2^2 + ... + U_n^2}}{U_1} \\ n = 1,2,3... \end{cases} \tag{9}$$

In equation (9), THD represents the total distortion rate of harmonic voltage.

The total distortion rate of harmonic voltage is calculated by Fourier function and periodic function, which eliminates the harmonic interference caused by nonlinear characteristics of electronic equipment.

2.1.2. Analysis of interference source on input side of frequency converter

In the main circuit of general frequency converter of electronic equipment in coal mine, the input side of frequency converter is diode rectifier and capacitor filter circuit. The rectifier is a non-linear device for the underground power grid, which will produce a lot of harmonic

Table 1
Switching mode of three-phase PWM inverter.

Serial number	Switch mode	Switch function ($S_aS_bS_c$)
1	$T'_a(D'_a), T'_b(D'_b), T'_c(D'_c)$	000
2	$T'_a(D'_a), T'_b(D'_b), T_c(D_c)$	001
3	$T'_a(D'_a), T_b(D_b), T'_c(D'_c)$	010
4	$T'_a(D'_a), T_b(D_b), T_c(D_c)$	011
5	$T_a(D_a), T'_b(D'_b), T'_c(D'_c)$	100
6	$T_a(D_a), T'_b(D'_b), T_c(D_c)$	101
7	$T_a(D_a), T_b(D_b), T'_c(D'_c)$	110
8	$T_a(D_a), T_b(D_b), T_c(D_c)$	111

interference at the grid side when it works [8]. Assuming that the input impedance of the converter is purely resistive and the filter capacitance is large enough, the current $i(t)$ at the input side of the converter can be obtained through analysis

$$i(t) = \sum_{n-1,3,5...}^{\infty} a'_n \sin(n\omega t) \tag{10}$$

In equation (10), a'_n represents the periodic voltage signals of the frequency converter, and its calculation equation is shown in equation (11):

$$\begin{cases} a'_n = \frac{4}{T}\int_0^{\frac{T}{2}} i(t)\sin(n\omega t)dt \\ = \frac{-4E_m}{n\pi R}[\frac{\sin(n-1)\theta_1}{n-1} + \frac{\sin(n+1)\theta_1}{n+1}] \\ n = 6k \pm 1 \\ k = 1,2,3,\ldots \end{cases} \tag{11}$$

In equation (11), E_m represents the peak value of the input line voltage of the frequency converter; R represents the input resistance of the frequency converter; θ_1 represents the phase angle of the fundamental current; k represents the random positive integer in the fundamental frequency.

It can be seen from equation (10) and equation (11) that the rectifier will produce strong components of high-order harmonic interference. The harmonic frequency is $6k \pm 1$ times of the fundamental frequency. There interference will affect the normal operation of other equipment through the public power line.

2.1.3. Analysis of interference source on output side of frequency converter

PWM technology is mostly used in the output side of the frequency converter of the electronic equipment in the coal mine. The three-phase PWM frequency converter uses comparator to compare the voltage signal with the triangle wave of the frequency modulated by the frequency converter to generate PWM pulse signal [9]. The output pulse voltage is generated by the power switch device. The typical rise time of IGBT is 50–100 ns. High speed power switching devices can accelerate the dynamic response process of inverter and improve the efficiency of inverter. However, the high frequency pulse signals generated by them have a high dv/dt, which can generate a considerable amount of pulse current through the stray capacitance to the ground of cable or motor [10]. The higher the switching frequency of IGBT is, the larger the dv/dt of the output voltage of the inverter is, and the larger the pulse current is. Because of the discrete sampling of power switch device and the nonlinearity of PWM modulation, the power spectrum of output voltage and current of frequency converter are discrete, and have the high-order harmonic and frequency conversion harmonic components corresponding to the switching frequency. In the three-phase voltage source inverter circuit, the switching mode of three-phase PWM inverter is shown in Table 1.

According to its switch mode, there are six IGBTs in the inverter circuit. If each IGBT is set as logic switch value, there may be eight logic switch combination states, which are described by logic switch function S_j, namely:

$$\begin{cases} S_j = \begin{cases} 1 & T_j or D_j \text{Conduction} \\ 0 & T'_j or D'_j \text{Conduction} \end{cases} \\ j = a,b,c \end{cases} \tag{12}$$

In equation (12), T_j represents parallel switch; D_j represents amplifier; a,b,c represents three-phase circuit; j represents number of logic switches [11].

In the three-phase voltage source inverter circuit, O is the equivalent neutral point of the DC side and N is the neutral point of the load motor. The following equation can be listed:

$$\begin{cases} V_{aN} = V_{aO} - V_{NO} \\ V_{bN} = V_{bO} - V_{NO} \\ V_{cN} = V_{cO} - V_{NO} \end{cases} \tag{13}$$

In equation (13), V_{aN}, V_{bN} and V_{cN} represent the neutral point voltage of the load motor of the three-phase circuit; V_{aO}, V_{bO} and V_{cO} represent the equivalent neutral point voltage of the DC side of the three-phase circuit; V_{NO} represent the voltage from the neutral point of the load motor to the equivalent neutral point of the DC side.

Under the condition of system symmetry:

$$V_{aN} + V_{bN} + V_{cN} = 0 \tag{14}$$

Three expressions in the equation are added to get:

$$V_{aO} + V_{bO} + V_{cO} = 3V_{NO} \tag{15}$$

The switch functions corresponding to the upper and lower pipes of the same bridge wall are complementary, then there are

$$\begin{cases} S'_j = 1 - S_j \\ j = a,b,c \end{cases} \tag{16}$$

In equation (16), S'_j represents another corresponding logic switch function on the same bridge wall [12].

From this, it can calculate:

$$\begin{cases} V_{jO} = S_j\frac{V_{dc}}{2} + (1-S_j)(-\frac{V_{dc}}{2}) = (2S_j - 1)\frac{V_{dc}}{2} \\ j = a,b,c \\ V_{NO} = \frac{V_{dc}}{6}\sum_{j=a,b,c} j = a,b,c \end{cases} \tag{17}$$

In equation (17), V_{jO} represents the output interference voltage of the inverter; V_{dc} represents the switching voltage of the three-phase voltage source inverter circuit.

It can be seen from equation (17) that the output interference voltage of the inverter is related to the switch function. The frequency spectrum of the interference voltage can be obtained by substituting the frequency spectrum of the switch function into equation (17). The frequency spectrum of the switch function is related to the PWM control mode. By analyzing the frequency spectrum of the switch function, it can get that the output interference of the inverter is mainly the high-order harmonic and its side frequency harmonic near the PWM switch frequency. The harmonic frequency is related to the switching frequency of the frequency converter. When the switching frequency is low, the human ear can hear the electromagnetic noise generated by the switching frequency. When the switching frequency is high, the human ear cannot hear it, but the high frequency signal still exists [13]. High frequency harmonic interference has become the main electromagnetic interference source in the mine, which constitutes the complex electromagnetic environment in the mine.

2.2. Overvoltage of motor terminal

2.2.1. Withstand voltage simulation of motor terminal

According to the theory of electromagnetic field, there are distributed resistance and distributed inductance in the transmission line. Distributed capacitance and distributed conductance due to imperfect insulation exist between conductors. When the switching frequency is very low, the wave length is longer than the line length, and these distribution parameters have little influence on the current and voltage transmitted on the line. The cable model can be represented by the centralized parameters. When the rise time reaches sub microsecond level, the rise edge of PWM pulse is rich in high frequency components. When the line length can be compared with the wave length, the distribution parameters of the line have a great influence on the current and voltage, so it is necessary to use the cable transmission line model of the distribution parameters to simulate the voltage borne by the motor terminals [14].

The specific steps are as follows: in the cable equivalent circuit, when a pulse voltage is applied at the end of the cable, the current begins to flow into the first inductance, and starts to charge the first capacitor, making its voltage E. Then, the current continues to flow through the next inductor and charges the next capacitor to a voltage of E. The instantaneous characteristic of the voltage can be described as a traveling wave. When the traveling wave reaches point x_1, the voltage on the capacitor towards the power supply side is E, and the voltage on the capacitor towards the motor side is 0. In transmission line theory, the traveling wave is called incident wave. When the incident wave is transmitted to the last capacitance C_n of the cable terminal and the charging voltage reaches E, there is still current on the last inductance L_n. Compared with the characteristic impedance of the cable, the impedance of the motor is very large, so the current on the inductance L_n continues to flow into the capacitance C_n until most of the stored energy is transferred to the capacitance C_n [15]. This will lead to an overload voltage on the capacitor C_n, the theoretical maximum value of which can be twice of the DC bus voltage. When the voltage on C_n reaches the maximum value $2E$, the reverse phase of current begins to return to the power side, and each capacitor is charged along the circuit to reach a higher voltage.

2.2.2. Analysis of voltage reflection process

The voltage reflection process is shown in Fig. 1, (a) shows the PWM pulse input at the cable sending end, and the motor terminal is considered as open circuit; (b) is the incident voltage wave and corresponding current wave; (c) is the reflected voltage wave and corresponding current wave of the motor terminal, because the motor terminal is equivalent to open circuit, the current is zero; (d) and (e) are the second incident wave and reflected wave, after the second reflection, the voltage and current wave propagate towards the inverter end, and then circulate continuously.

In the process of voltage reflection, the reflection coefficient of motor terminal is:

$$\Gamma_L = \frac{R_L - Z_0}{R_L + Z_0} \tag{18}$$

In equation (18), Γ_L is the reflection coefficient of motor terminal; R_L represents impedance of load terminal; Z_0 represents cable's characteristic impedance [16].

The reflection coefficient of inverter terminal is:

$$\Gamma_S = \frac{R_S - Z_0}{R_S + Z_0} \tag{19}$$

In equation (19), R_S represents the source impedance; Γ_S represents the reflection coefficient of the inverter terminal. The transmission time t_t of the output pulse in the long cable is:

$$t_t = \frac{l_c}{v} \tag{20}$$

In equation (20), l_c represents cable length; v represents pulse speed.

According to the transmission line theory, in the at time period, the forward traveling wave of the inverter's output pulse and the reverse traveling wave amplitude of the motor terminal are both positive. Because of $R_L \approx Z_0$, it can be seen from equation (18), $\Gamma_L \approx 1$, in this process, the motor terminal voltage is approximately doubled. At the time of $t = 2t$, the reverse traveling wave reaches the inverter terminal and reflects. Since $R_S \ll Z_0$, according to equation (19), $\Gamma_S \approx -1$, the reflected wave with negative amplitude will be generated to the motor terminal. Since the terminal voltage of the motor starts to decrease in $2t_t - 3t_t$, the peak value of the terminal line voltage of the motor is the sum of the total voltage generated at the motor terminal after the inverter's output pulse is transmitted through the cable three times and the amplitude of the inverter's output pulse voltage.

2.3. Realization of anti-electromagnetic interference mining of underground electronic equipment in coal mine

Based on the network communication technology, the supporting equipment of the comprehensive mining face is designed to realize the anti-electromagnetic interference mining of the underground electronic equipment. The mining process of the designed supporting equipment of the fully mechanized coal face is as follows: firstly, the coal is broken down from the whole coal seam, then the broken coal is loaded into the transportation equipment of the working face, and the coal is transported out of the working face through the transportation equipment [17]. In order to maintain enough space in the working face, it is necessary to support the stope with support. Finally, it is necessary to deal with the roof of goaf to reduce the effect of mine pressure on the stope.

The designed supporting equipment of the fully mechanized working face adopts the high-power coal cutter to realize the coal falling and loading, and the powerful bendable scraper conveyor to realize the coal transportation. The movable hydraulic support is used to support the roof, so that the mining process of the working face is fully mechanized [18]. During the fully mechanized mining, the equipment and working procedures are closely linked, which can achieve continuous operation, high production, high efficiency, safe operation and other effects. The equipment and layout of the fully mechanized working face are shown in Fig. 2 [19].

In order to transport the coal out of the working face, crusher, transfer machine and retractable belt conveyor should be installed in the transport lane of the working face. After the coal on the scraper conveyor of the working face is crushed by the crusher, the transfer machine and transport equipment will transport the coal out of the working face. In addition, in order to reduce the coal dust on the working face, it is necessary to configure the spray pumping station and the emulsion pump station providing hydraulic support power.

3. Experimental test

3.1. Experimental design

In this paper, the mining method of anti-electromagnetic interference for underground electronic equipment in coal mine considering network communication technology is tested. Longgu Coal Mine is selected as the experimental coal mine. Longgu Coal Mine is located in the south central part of Juye Coal field. The 3# coal seam currently mined belongs to rich coal, with a coal seam dip angle of 3–13° (average 8.0°), the average thickness of coal seam of 8.5 m, mining height of 3.7 m, caving coal of 4.2 m. The layout of the existing working face of Longgu Coal Mine is shown in Fig. 3.

The current 2303 working face has a dip length of 270 m and a strike length of 2200 m, and adopts downward ventilation. The roadway along the goaf is with width of 5 m and height of 4 m, and the wall is supported by bolting and shotcreting. The working face belongs to

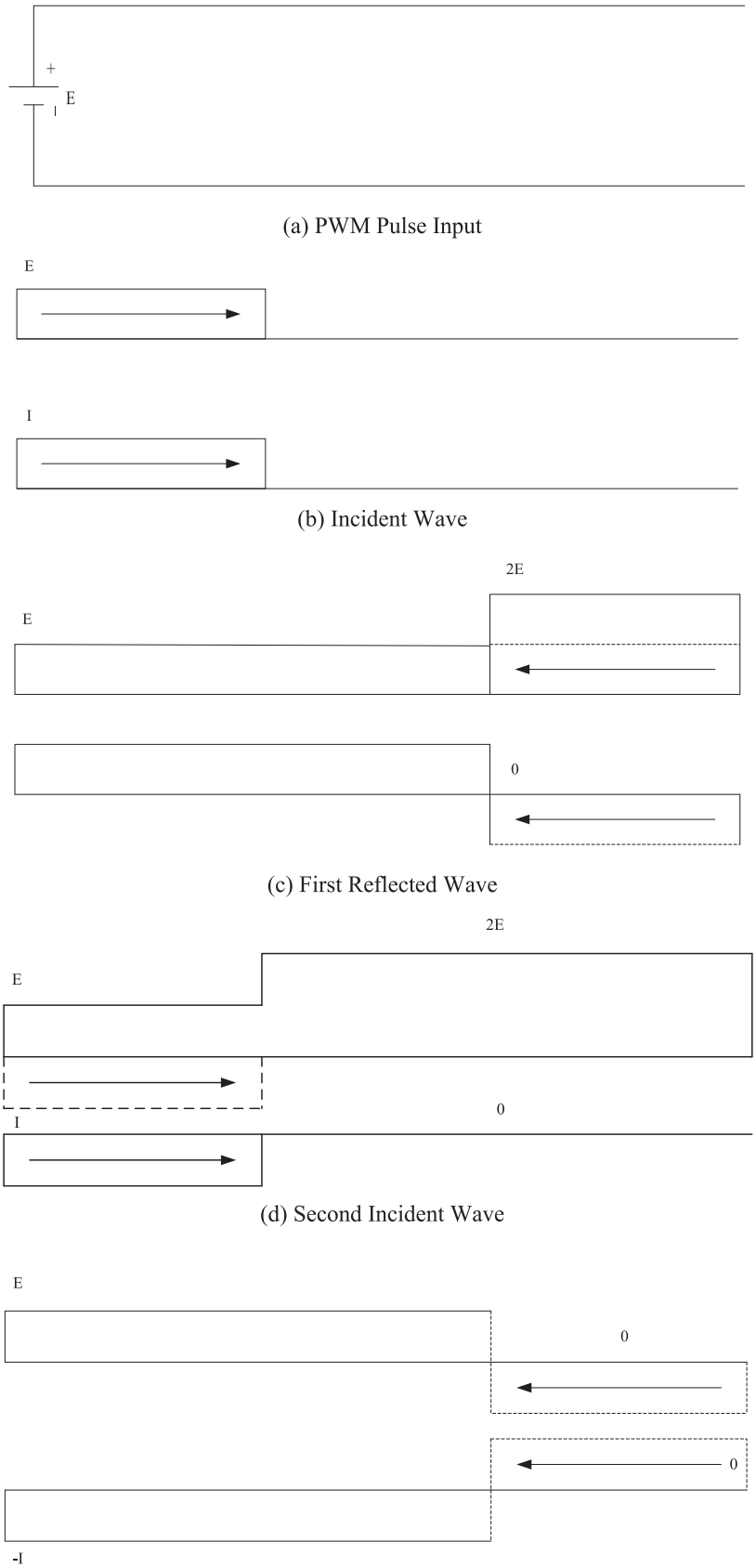

Fig. 1. Voltage reflection process.

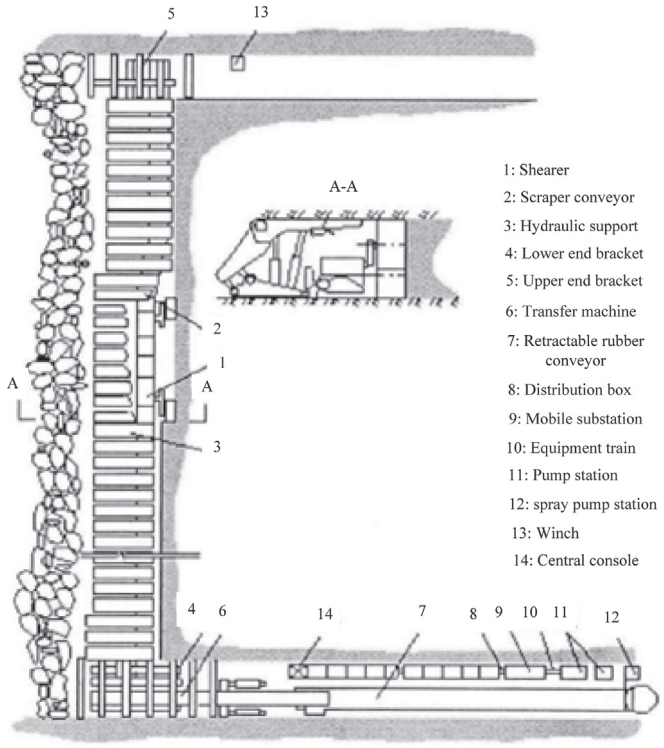

Fig. 2. Equipment and layout of fully mechanized working face.

deep and high temperature coal mining, and the electromagnetic interference of electronic equipment is serious.

The underground electronic equipment in the experiment includes frequency converter, cable, motor and output filter. The specific parameters of frequency converter, cable and motor are shown in Table 2.

The specific parameters of the output filter are shown in Table 3.

The pulse voltage waveform of the output filter is shown in Fig. 4.

The layout of network communication nodes in the coal mine is as follows: there are three Mesh nodes. Mesh node adopts Strix's indoor wireless system node. Each Mesh node includes five parts: antenna module, user connection module, network connection module, network server module and basic module. The network connection module works at 5.8 GHz, and the user access module works at 2.4 GHz. The three nodes are named Mesh Point l, Mesh Point 2 and Mesh Point 3 respectively. Table 4 shows the configuration of three Mesh nodes.

In this paper, the anti-electromagnetic interference mining method of underground electronic equipment by considering network communication technology is used to carry out the anti-electromagnetic interference mining experiment of underground electronic equipment in this coal mine. Five groups of experiments were set, each group was repeated 10 times, and 50 M data was transmitted. According to the wireless transmission rate of downhole data when the transmission time of output pulse was in the range of 0.5 μs-1.1 μs, the experimental results were taken as experimental results. In order to prevent the lack of contrast between the experimental results, two original mining methods of anti-electromagnetic interference for underground electronic equipment in coal mine are used as comparative experimental methods, including the mining method of anti-electromagnetic interference for underground electronic equipment in coal mine based on electric field shielding technology and the mining method of anti-electromagnetic interference for underground electronic equipment in coal mine based on single point grounding technology. The two methods are also used to mine the electronic equipment of the coal mine against electromagnetic interference, and the wireless transmission rate of downhole data when the transmission time of the output pulse is in the range of 0.5 μs–1.1 μs is used as the comparison experimental data.

3.2. Analysis of experimental results

When the transmission time of the output pulse is in the range of 0.5 μs–0.7 μs, the experimental data of wireless transmission rates of the three methods are shown in Table 5.

According to the comparison experimental data of the wireless transmission rate of downhole data when the transmission time of output pulse is in the range of 0.5 μs–0.7 μs in Table 5, it can be seen that the wireless transmission rate of underground data in the mining method of anti-electromagnetic interference for underground electronic equipment considering network communication technology is higher than that in the mining method of anti-electromagnetic interference for underground electronic equipment based on electric field shielding technology and single point grounding technology.

When the transmission time of output pulse is in the range of 0.71 μs–0.9 μs, the comparison experimental data of wireless transmission rate in the mining method of anti-electromagnetic interfer-

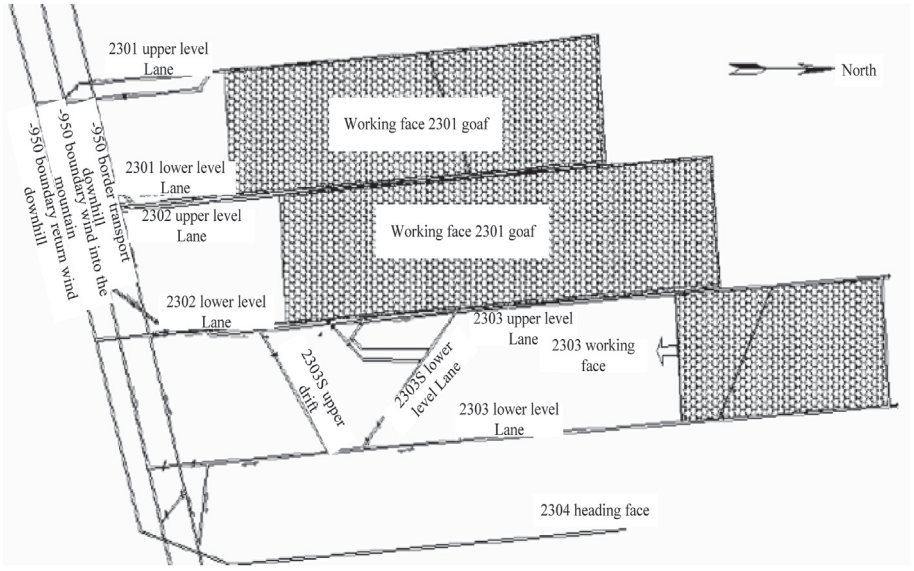

Fig. 3. Layout of existing working face in Longgu coal mine.

Table 2
Specific parameters of frequency converter, cable and motor.

Converter parameters	DC Bus Voltage	1000 V
Switching frequency	2 kHz	
Carrier frequency	2 kHz	
Fundamental frequency	50 Hz	
Cable distribution parameters	Inductance per unit length	0.362 μH
Capacitance per unit length	0.01 nF	
Characteristic impedance	189Ω	
Cable length	100 m	
Motor parameters	Reflection coefficient of motor terminal	0.9
Motor power	5 kW	

Table 3
Specific parameters of output filter.

Output filter	R (Ω)	C (μF)		L (mH)	
RC filter of motor terminal	30	1.2			
Inverter's output RLC filter	190	0.1		0.07	
Inverter's output LC-RLC cascade filter	35	LC	RLC	LC	RLC
4	10	1.6	3		

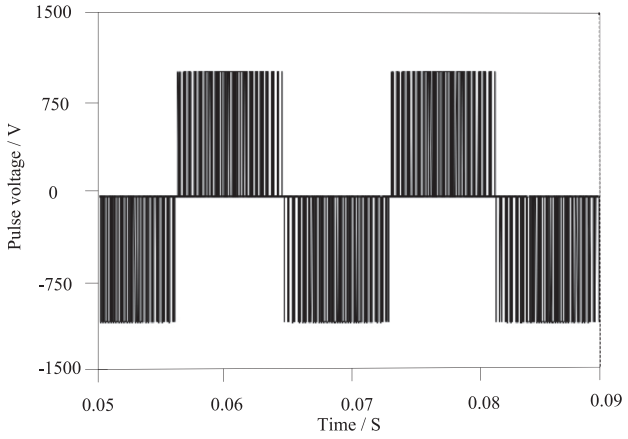

Fig. 4. Pulse voltage waveform of output filter.

ence for underground electronic equipment in coal mine considering network communication technology and the mining methods of anti-electromagnetic interference for underground electronic equipment in coal mine based on electric field shielding technology and single point grounding technology are shown in Table 6.

According to the comparison experimental data of the wireless transmission rate of downhole data when the transmission time of output pulse is in the range of 0.71 μs–0.9 μs in Table 6, it can be seen that the wireless transmission rate of underground data in the mining method of anti-electromagnetic interference for underground electronic equipment considering network communication technology is higher than that in the mining method of anti-electromagnetic interference for underground electronic equipment based on electric field shielding technology and single point grounding technology.

When the transmission time of output pulse is in the range of 0.91 μs–1.1 μs, the comparison experimental data of wireless transmission rate in the mining method of anti-electromagnetic interference for underground electronic equipment in coal mine considering network communication technology and the other two mining methods of anti-electromagnetic interference for underground electronic equipment in coal mine are shown in Table 7.

According to the comparison experimental data of the wireless transmission rate of downhole data when the transmission time of output pulse is in the range of 0.91 μs–1.1 μs in Table 7, it can be seen that the wireless transmission rate of underground data in the mining method of anti-electromagnetic interference for underground electronic equipment considering network communication technology is higher than that in the mining method of anti-electromagnetic interference for underground electronic equipment based on electric field shielding technology and single point grounding technology.

According to the above experimental results, when the transmission time of the output pulse is in the range of 0.5 μs–1.1 μs, the wireless data transmission rate of the mining method of anti-electromagnetic interference for underground electronic equipment considering network communication technology is always higher than that of the mining methods of anti-electromagnetic interference for underground electronic equipment based on electric field shielding technology and single point grounding technology.

Table 4
Configuration of three mesh nodes.

Node name 5.8G Hz	IP address 5.8G Hz	Working channel 5.8G Hz	Working mode 5.8G Hz	Working channel	Working mode
MeshPointl	192.168.1.154	N/A	NS	N/A	N/A
192.168.1.48	5825	CC	1	CC	
MeshPoint2	192.168.1.49	5825	NC	6	CC
192.168.1.153	5500	CC	11	CC	
MeshPoint3	192.168.1.47	5500	NC	1	CC
192.168.1.46	5745	CC	6	CC	

Table 5
Comparison Experimental Data of the Wireless Transmission Rate of Down Hole Data When the Transmission Time of Output Pulse is in the Range of 0.5 μs–0.7 μs.

The transmission time of output pulse (μs)	Wireless transmission rate of downhole data (bit/s)		
Method of considering network communication technology	Method based on single point grounding technology	Method based on single point grounding technology	Method based on single point grounding technology
0.50	0.236	0.169	0.212
0.51	0.254	0.189	0.196
0.52	0.269	0.138	0.194
0.53	0.214	0.185	0.198
0.54	0.229	0.136	0.189
0.55	0.238	0.132	0.136
0.56	0.221	0.185	0.134
0.57	0.201	0.158	0.186
0.58	0.201	0.139	0.128
0.59	0.214	0.128	0.136
0.60	0.214	0.185	0.147
0.61	0.254	0.128	0.139
0.62	0.236	0.169	0.189
0.63	0.286	0.136	0.168
0.64	0.274	0.158	0.174
0.65	0.275	0.139	0.136
0.66	0.236	0.178	0.124
0.67	0.284	0.193	0.198
0.68	0.225	0.187	0.187
0.69	0.214	0.158	0.135
0.70	0.298	0.251	0.148
Mean value	0.24157	0.16386	0.16448

Table 6
Comparison Experimental Data of the Wireless Transmission Rate of Down Hole Data When the Transmission Time of Output Pulse is in the Range of 0.71 μs–0.9 μs.

The transmission time of output pulse (μs)	Wireless transmission rate of downhole data (bit/s)		
Method of considering network communication technology	Method based on single point grounding technology	Method based on single point grounding technology	Method based on single point grounding technology
0.71	0.246	0.139	0.139
0.72	0.258	0.178	0.178
0.73	0.201	0.177	0.199
0.74	0.208	0.189	0.187
0.75	0.296	0.147	0.188
0.76	0.286	0.147	0.174
0.77	0.289	0.149	0.130
0.78	0.288	0.156	0.128
0.79	0.208	0.139	0.118
0.80	0.274	0.120	0.125
0.81	0.274	0.174	0.114
0.82	0.218	0.174	0.119
0.83	0.296	0.149	0.174
0.84	0.268	0.178	0.186
0.85	0.268	0.189	0.132
0.86	0.235	0.196	0.147
0.87	0.258	0.201	0.175
0.88	0.268	0.199	0.175
0.89	0.264	0.149	0.198
0.90	0.261	0.187	0.174
Mean value	0.2582	0.16685	0.158

In this paper, by analyzing the harmonic interference sources, the motor terminals are treated with overvoltage, which effectively eliminates the electromagnetic interference, reduces the redundancy of calculation, and makes the data transmission of electronic equipment in coal mine have high speed and anti-interference.

4. Conclusions

With the rapid development of high-power power electronic technology and the wide application of frequency conversion equipment in the coal mine, the problems of harmonic and electromagnetic interference are paid more and more attention. It has important theoretical research significance and practical application value to study the mining method of anti-electromagnetic interference for underground electronic equipment in coal mine. In this paper, the interference source is analyzed and the adverse effects caused by harmonic interference are eliminated, When the output pulse transmission time is in the range of 0.5 μs–1.1 μs, the method designed in this paper can improve the wireless transmission rate of underground data. In this study, the bit error rate after data transmission is not considered. In future experi-

Table 7
Comparison Experimental Data of the Wireless Transmission Rate of Down Hole Data When the Transmission Time of Output Pulse is in the Range of 0.91 μs–1.1 μs.

The transmission time of output pulse (μs)	Wireless transmission rate of downhole data (bit/s)		
Method of considering network communication technology	Method based on single point grounding technology	Method based on single point grounding technology	Method based on single point grounding technology
0.91	0.230	0.119	0.129
0.92	0.258	0.123	0.168
0.93	0.269	0.167	0.149
0.94	0.281	0.189	0.196
0.95	0.246	0.197	0.132
0.96	0.268	0.196	0.159
0.97	0.291	0.185	0.158
0.98	0.298	0.156	0.157
0.99	0.288	0.179	0.118
1.00	0.247	0.108	0.165
1.01	0.274	0.104	0.142
1.02	0.208	0.139	0.148
1.03	0.287	0.191	0.139
1.04	0.220	0.198	0.186
1.05	0.210	0.107	0.129
1.06	0.291	0.193	0.187
1.07	0.282	0.231	0.165
1.08	0.267	0.190	0.172
1.09	0.263	0.148	0.104
1.10	0.260	0.178	0.162
Mean value	0.2619	0.1649	0.15325

ments, further research on the accuracy of data transmission of electronic equipment in coal mines is needed to improve the practicability of the designed method.

CRediT author statement

Yapeng Yan: Conceptualization, Writing- Original draft preparation, Methodology, Software. **Wentao Cao:** Data curation, Writing-Reviewing and Editing, Validation.

Declaration of competing interest

The authors declare that they have no known competing financial interests or personal relationships that could have appeared to influence the work reported in this paper.

References

[1] X. Wen-Quan, Research on the failure of the hydraulic system of the mechanical electronic equipment of the nonferrous metal mine, World Nonferrous Met. (2018).
[2] O.U. Hai-Bo, H.F. Amp, Fault diagnosis technology of mine electronic and electrical equipment, World Nonferrous Met. (2018).
[3] Y. Lin, L. Meng, C. Jin, L. Shuang, Design and anti-interference ability analysis of RFID positioning system for mine locomotive, in: IEEE International Conference on Computational Intelligence and Computing Research (ICCIC), 2017, pp. 1–4.
[4] L. Wang, Y. Wang, J. Pei, Coal mine ventilator remote monitoring system based on the fuzzy control, in: Proceedings of the 2012 International Conference on Communication, Electronics and Automation Engineering, 2013, pp. 181–186.
[5] X. Gao, H. Jia, Z. Chen, Anti-jamming method of OFDM wide-band measuring and controlling based on adaptive sensing, Syst. Eng. Electron. 42 (488) (2020) 204–210.
[6] A.M. Kettner, M. Paolone, A generalized index for static voltage stability of unbalanced polyphase power systems including Thévenin equivalents and polynomial models, IEEE Trans. Power Syst. 34 (6) (2019) 4630–4639.
[7] R. Bhosale, V. Agarwal, Fuzzy logic control of the ultracapacitor interface for enhanced transient response and voltage stability of a DC microgrid, IEEE Trans. Ind. Appl. 55 (1) (2018) 712–720.
[8] S. Maharjan, D.S. Kumar, A.M. Khambadkone, Enhancing the voltage stability of distribution network during PV ramping conditions with variable speed drive loads, Appl. Energy 264 (2020) 114733.
[9] I. Nikoloska, N. Zlatanov, Z. Hadzi-Velkov, Capacity of a full-duplex wirelessly powered communication system with self-interference and processing cost, IEEE Trans. Wireless Commun. 17 (11) (2018) 7648–7660.
[10] N.M. Gowda, A. Sabharwal, CPLink: interference-free reuse of cyclic-prefix intervals in OFDM-based networks, IEEE Trans. Wireless Commun. 18 (1) (2018) 665–679.
[11] S. Kusaladharma, Z. Zhang, C. Tellambura, Interference and outage analysis of random D2D networks underlaying millimeter-wave cellular networks, IEEE Trans. Commun. 67 (1) (2018) 778–790.
[12] L. Liang, Y. Wang, Y. Hu, W. Chen, Z. Yan, Protection of electronic circuit based on YBCO superconducting thin film against the induced current interference, IEEE Trans. Appl. Supercond. 29 (6) (2019) 1–6.
[13] R.A. Rodin, K.Y. Sakharov, V.A. Turkin, O.V. Mikheev, Measuring complex for the evaluation of the immunity of radioelectronic equipment to the noise of pulsed electromagnetic radiation, Meas. Tech. 61 (9) (2018) 937–940.
[14] K.W. Park, C. Park, Determination of LO frequency for reception of maximum number of GNSS signals in presence of interference, Electron. Lett. 55 (9) (2019) 552–554.
[15] R.A. Rodin, K.Y. Sakharov, V.A. Turkin, O.V. Mikheev, Measuring complex for the evaluation of the immunity of radioelectronic equipment to the noise of pulsed electromagnetic radiation, Meas. Tech. 61 (9) (2018) 937–940.
[16] P. Gao, Q. Ma, D. Ding, D. Wang, X. Lou, T. Zhai, F. Xia, Distinct functional elements for outer-surface anti-interference and inner-wall ion gating of nanochannels, Nat. Commun. 9 (1) (2018) 1–11.
[17] Q. Kang, Q. Zhang, L. Zang, M. Zhao, X. Chen, D. Shen, Enhancement anti-interference ability of photoelectrochemical sensor via differential molecularly imprinting technique demonstrated by dopamine determination, Anal. Chim. Acta (2020) 201–209.
[18] C. Chen, Z. Shang, F. Zhang, H. Zhou, J. Yang, D. Wang, X. Mu, Dual-mode resonant infrared detector based on film bulk acoustic resonator toward ultra-high sensitivity and anti-interference capability, Appl. Phys. Lett. 112 (24) (2018) 243501.
[19] D. Liu, L. Guo, Y. Wu, H. Lv, G. Xu, Anti-interference function of scale-free spiking neural network under AC magnetic field stimulation, IEEE Trans. Magn. (2020) 1–5.